

# SELECTED APPLICATIONS OF ELECTRON BEAMS IN SOLID STATE MATERIALS AND DEVICES TECHNOLOGY

S. C. JAIN

Solid State Physics Laboratory, Delhi-110007

(Received 11 January 1980)

Experimental work on electron beam annealing of implanted or diffused semiconductor layers is reviewed. In the pulsed beam annealing technique, the top layer of the semiconductor melts and regrows epitaxially. All dopant atoms are frozen in electrically active state during this process. The point defects and clusters caused by radiation damage are completely annealed out. The bulk of the material remains unaffected as its temperature does not rise by more than a few degrees. In the CW electron beam annealing, the layer does not melt but due to sharp temperature gradient and high temperature of the layer, the growth of solid phase epitaxial layer is induced. However, a part of the dopant atoms may remain electrically inactive in this process of annealing. The pulsed beam annealing has also been used for growing high quality single crystal layers of germanium on silicon substrate. Recently, a new technology has been developed to grow silicon single crystal layers on amorphous substrates. Recent advances in the method of determination of lifetime using electron beams are also discussed.

Work on Electron beam<sup>1</sup> (E-beam) annealing of defects in crystals was done in 1974 and similar work on laser beam<sup>2</sup> annealing, in 1975. Extensive work has now been done in this field and it has been shown that the results obtained by E-beam annealing are practically identical to those obtained by laser annealing<sup>3,4</sup>. E-beam annealing, however, offers some advantages<sup>5</sup>. In this paper we review the field and discuss the characteristics of devices like bipolar transistors, MOS devices and Solar Cells fabricated by ion implantation and E-beam annealing techniques. To assess the potential of the technique and for the sake of completeness, results of laser annealing have also been included.

Electron beams have been used as tools for investigating the quality of crystals for a long time e.g. Electron microscopy, ESCA and Auger spectrometers and electron probes. These techniques have not been mentioned in this paper. However, use of electron beams to determine lifetime in *p-n* junction devices has been discussed, since considerable advances in this technique have been made recently<sup>6-8</sup>.

Another modern application of E-beam is electron lithography which is playing a very significant role in increasing the density of components on a chip leading to VLSI technology. Considerable improvements in our understanding of proximity effects, in developing new resists, masks and dry plasma etching technique have been made<sup>9</sup>. Some other applications of E-beams, viz., use of electron beam in pumping lasers, free electron lasers<sup>10</sup> and fabrication of fresnel zone plates<sup>11</sup> for focussing soft X-rays have been excluded from the scope of this article. Other applications selected for discussion in this paper are liquid phase epitaxy, solid phase epitaxy, grapho-epitaxy, defect annealing, dopant dispersion, polysilicon gates, high voltage diodes III-V compound devices and lifetime measurements.

## ELECTRON AND LASER BEAM ANNEALING

### *Advantages of E-beam Annealing*

It is well known that as a technique, ion implantation is much superior to diffusion for making several special types of devices. In many cases, ion implanted devices have superior characteristics and/or are much cheaper. The process of ion implantation, however, is accompanied by the production of a large number of point defects and their clusters. The implanted devices have to be annealed at very high temperatures to anneal out these defects. The impurities get redistributed during this process of annealing and other undesirable effects occur. Moreover, the annealing is never completely effective in removing the defects unless the implanted layer is so heavily damaged that it becomes amorphous.

All these problems disappear if the annealing is done by exposing the implanted layer to short high power pulses of E-beams or scanning with a CW E-beam. Since only the thin implanted layer is heated for a short time during this process, it avoids plastic deformation of the bulk material, degradation of lifetime, auto doping or out doping. The concentration of the implanted dopant is insensitive to the presence of dislocations and grain boundaries and large areas can be implanted. This type of annealing is important even in the diffused layers when the dopant concentration is very high and clusters and pairs of impurities and other defects are formed. Thermal annealing is quite ineffective in such cases but E-beam annealing restores complete atomic dispersion and electrical activity in the layers. In addition to the important role

it is playing in the area of device fabrication, it is likely to play a very significant role in VLSI technology in the near future.

Many workers have reported that the results of E-beam and laser beam annealing are practically identical. Tables 1 and 2 give the comparative characteristics of laser and E-beam annealing techniques.

TABLE 1  
PULSED ELECTRON BEAM VS PULSED LASER ANNEALING<sup>5</sup>

Characteristic	Electron beam	Lasers
Pulsewidth	10-200 ns	10-130 ns
Absorption	Material density	$\lambda, T, \alpha$ (Surface)
Beam control	Elec. Mag. Fields	Optical
Diameter	To 76 mm (Si)	30 $\mu\text{m}$ to 20 mm (Si)
Uniformity :		
Macroscopic	$\pm 5\%$	Gaussian profile
Microscopic	Self-field improves	Hotspots, Diffraction
Fluence	$> 1 \text{ Joule/cm}^2$	1-10 Joules/cm <sup>2</sup>
Processing depth	Controllable	Maximum $< 1 \mu\text{m}$
Wafer surface	Remains flat	Becomes 'Furrowed'
Environment	Vacuum	Air or Vacuum
Throughput	$> 1 \text{ Wafer/Min.}$	?
Limitation	Residual charge	Oxide film interference unstable heating for small $\alpha$

TABLE 2  
PULSED VS CW SCANNING E-BEAM OR LASER ANNEALING<sup>4,5</sup>

	Pulsed	CW scanning
Laser	Q switched ruby or Nd : YAG 10-130 ns, 1-10 J/cm <sup>2</sup>	Ar or Kr, 7 watts, 0.2 W/ $\mu\text{m}$ , 2.8 cm/sec
E-Beams	10-200 ns, $> 1 \text{ J/cm}^2$	30 kV, 0.5 mA, 0.2 W/ $\mu\text{m}$ , 2.5 cm/sec
Crystallization	Liquid phase epitaxy	Solid phase epitaxy
Dopant	Redistribution	No redistribution
Electrical activity	Complete even if concentration is more than solubility limit	Complete only if concentration is less than solubility limit
Profile	No theory	Theory agrees with experiment

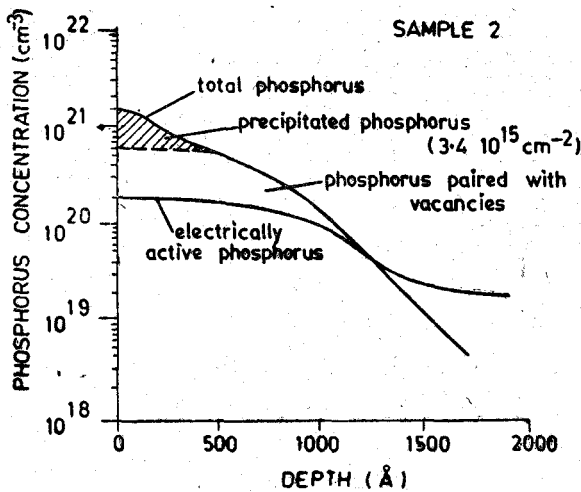


Fig. 1—Concentration of phosphorus in a heavily diffused silicon wafer is plotted as a function of depth. The shaded area gives the concentration of clustered or precipitated phosphorus determined by RBS technique.

Annealing of Thermally Diffused or Implanted Layers

Secondary Ion Mass Spectrometry (SIMS), Rutherford Back Scattering (RBS) and Hall and conductivity measurements can be used to measure concentrations of dopant present in different states. The results<sup>12,13</sup> of such measurements of a silicon layer heavily diffused with phosphorus are shown in Fig. 1. The total phosphorus concentration is obtained by SIMS data whereas the fraction present in the form of interstitial clusters or precipitates is obtained by RBS data in channelling conditions. Electrically active phosphorus is determined by Hall and conductivity measurements. The concentration of phosphorus paired with vacancies is obtained by subtracting from the total phosphorus concentration, the fraction present in the form of precipitates and in the form of electrically active phosphorus.

The effect of laser irradiation annealing on the

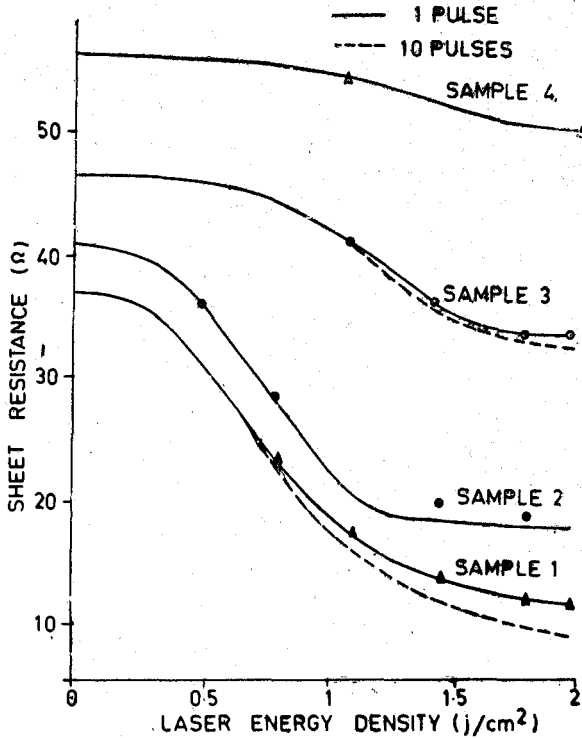


Fig. 2—Effect of pulsed laser annealing on the sheet resistance of a similar silicon wafer is shown as a function of the energy of the pulsed laser used for annealing.

E-beam or laser annealing has been more extensively used in implanted layers. In addition to dispersing the dopant atoms substitutionally and making them electrically active as in the case of diffused layers discussed above, point defects and their aggregates due to radiation damage are completely annealed out by this process.

The impurity distribution in a CW E-beam annealed arsenic implanted silicon layer is shown<sup>14</sup> in Fig. 4. The distribution was measured by stripping and van der Pauw method. The measured mobility

sheet resistance of this layer is shown in Fig. 2. It will be seen that the decrease in sheet resistance on laser annealing is more pronounced in samples 1 and 2, which are more heavily doped and if the laser energy is high, repeated pulses give a small amount of additional annealing. Fig. 3 shows that on pulsed laser annealing the concentration of phosphorus near the surface diminishes and depth to which phosphorus has diffused increases. The precipitates and the clusters dissolve mainly because of this redistribution of phosphorus. The pairs also dissolve increasing the concentration of active phosphorus. The phosphorus exists wholly in the dissolved and electrically active state because of the fastness of the rate at which annealing is done. This conclusion is supported by a separate experimental<sup>12,13</sup> observation involving thermal annealing of the laser annealed samples at 700°C. The sheet resistance increases by 50 percent in about 5 minutes, indicating that some of the dissolved electrically active phosphorus again forms pairs, clusters or precipitates.

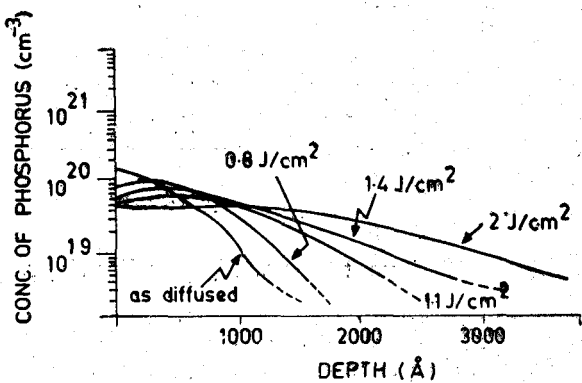


Fig. 3—Effect of laser pulse annealing on the distribution of the phosphorus concentration in a silicon wafer is shown as a function of depth for different pulse energies. The redistribution takes place because the diffused layer melts [and regrows epitaxially during the pulse annealing process.

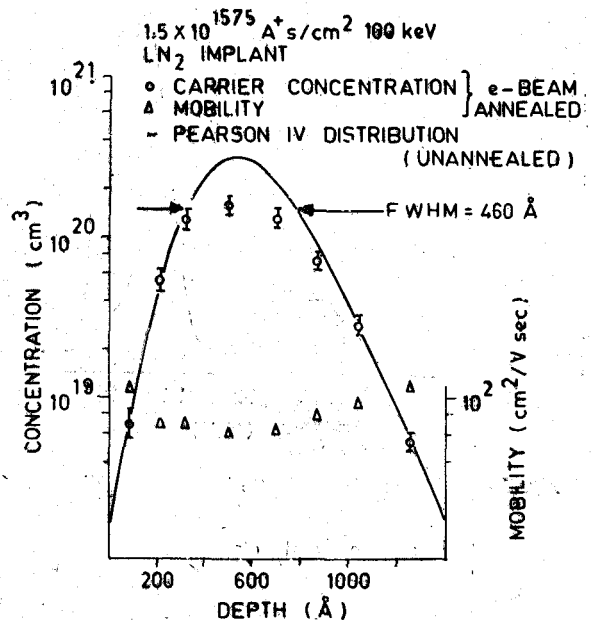


Fig. 4—Measured distribution of electrically active phosphorus in an implanted and CW electron beam annealed silicon wafer is compared with the theoretical distribution. The results of measured mobility are also shown.

results are also shown. A comparison of these results with the theoretical results (solid curve) show that there is no redistribution of the impurity during the annealing by CW scanning E-beams. The small discrepancy near the peak is presumably due to inactivity of some arsenic which may still be present in the form of pairs. This result is to be contrasted with the result of pulsed beam annealing discussed earlier, where redistribution and complete restoration of electrical activity were obtained.

### Annealing through Oxide Films

Recent work has shown that electron beam pulses can be used to anneal implant damages beneath thin oxide layers or through windows in thick oxide<sup>5</sup>. This is important since integrated circuit fabrication require annealing ion implants in oxide masked patterns. The results given in Table 3 show that effect of window size in 0.6 micron thick oxide on a 30 keV B implant to a level of  $2 \times 10^{15}$  ions/cm<sup>2</sup> is negligible. Because of the large fluence in the pulse, a high transient conductivity is induced even in the best insulator and charge is conducted to the ground. No charging of the oxide layer occurs.

### Epitaxy

A short (0.1 micro-sec) pulse of high energy high fluence E-beam produces a temperature exceeding the melting point of the material. Cooling and recrystallization begins at the interface and this results in the epitaxial regrowth of excellent quality single crystal layer. It is due to this process that redistribution of dopant takes place and even a very large concentration of dopant is frozen in electrically active state as discussed earlier. The helium ion back scattering (RBS) data shows (Fig. 5) that a 0.26 micron layer of evaporated germanium over single crystal silicon grew epitaxially<sup>5</sup> into a monocrystalline layer by electron pulse beam processing. Electron microscopy studies show some dislocations at the interface which is usual in such cases of hetero-epitaxy due to lattice mismatch. Thus 0.1 to 3 micron of high purity epitaxial layers can be grown in this manner. Zone purification takes place during the regrowth. The concentration distribution of arsenic or phosphorus, if present within solid solubility limit, is only slightly affected but the concentration of heavy metal impurities near the surface increases.

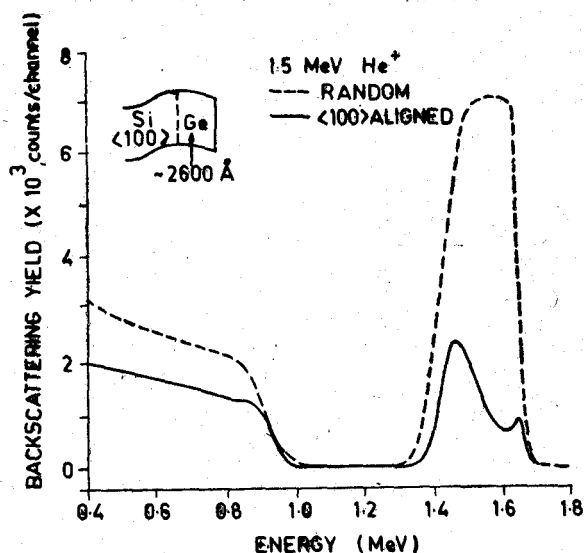


Fig. 5—Rutherford Back Scattering (RBS) Helium Ion Spectra of Ge film on silicon substrate after pulsed electron beam annealing. This spectra and electron microscopy experiments show that the regrown single crystal epitaxial Ge films are better as compared to those which can be achieved with furnace processing.

TABLE 3

SHEET RESISTANCE <sup>5</sup> OF STRUCTURES FORMED BY PULSE ANNEALING THROUGH OXIDE WINDOWS	
Width of window (microns)	Sheet resistance (ohms/square $\pm 20\%$ )
5.0	286
12.5	236
50	230

Electron microscopy studies show some dislocations at the interface which is usual in such cases of hetero-epitaxy due to lattice mismatch. Thus 0.1 to 3 micron of high purity epitaxial layers can be grown in this manner. Zone purification takes place during the regrowth. The concentration distribution of arsenic or phosphorus, if present within solid solubility limit, is only slightly affected but the concentration of heavy metal impurities near the surface increases.

If the electron beam parameters are chosen so that the surface layer does not melt, the large temperature gradient and high temperature still force epitaxial regrowth.

A new technique to grow high quality single crystal silicon films on amorphous substrates has been developed<sup>15</sup> by Gens. *et al.* A grating is made on amorphous fused silica using photo-lithographic techniques. The grating has a square wave cross section with a 3.8 micron spacing and 100 nm depth. The

amorphous silicon deposited on the grating is recrystallised using laser or electron beams. Fig. 6 illustrates the procedure used by Gens. *et al.* High quality single crystal layers are obtained on amorphous substrates by this process, known as grapho-epitaxy.

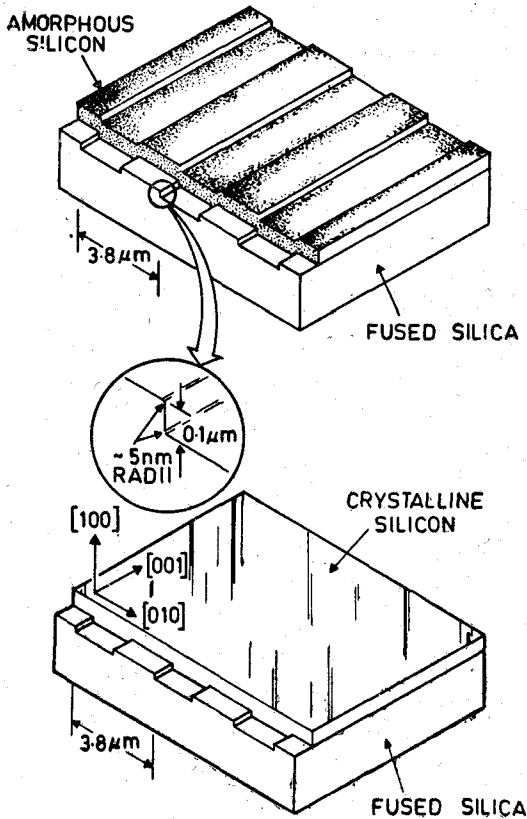


Fig. 6—Schematic diagram of the method developed for grapho-epitaxy to obtain good quality single crystal silicon films on fused silica substrates.

### Polysilicon Gates

In many CCD and other MOS devices, polysilicon is used for gates and interconnections. The sheet resistance of the material is an important characteristic for device operation. Since the gate in a CCD designed for imaging has to be transparent, the sheet resistance must be kept small without unduly increasing the thickness of the material. A short electron pulse at a fluence level of 0.7 joule/cm<sup>2</sup> results in the

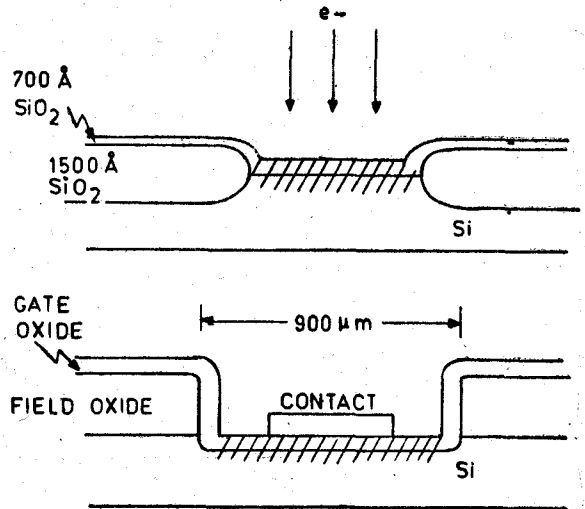


Fig. 7—MOS structure formed by implantation and pulled electron beam annealing through an oxide layer.

reduction of the sheet resistivity of the polysilicon by a factor of two from the typical values achieved with furnace processing but no other damage is caused<sup>5</sup>. Gibbons *et al.* have studied both the thermally annealed and CW scanned laser annealed polysilicon films<sup>14</sup>. A 0.5 micron polysilicon layer was deposited on Si<sub>3</sub>N<sub>4</sub> by CVD method. The layer was implanted with 60 keV B to a level of 5 × 10<sup>14</sup> ions/cm<sup>2</sup> giving a B concentration of 10<sup>19</sup>/cm<sup>3</sup>. One sample was thermally annealed for half an hour at 1000°C in flowing nitrogen. The measured values of some important properties of this sample are 4.7 × 10<sup>14</sup>/cm<sup>2</sup> for carrier concentration, 623 ohm/square for sheet resistance, 24 cm<sup>2</sup>/Vsec for mobility and 0.1 micron for the grain size. Another sample was annealed by a CW 11 watt argon laser with a scan rate of 12.5 cm/sec. The sample temperature was 350°C. The measured values of the properties of this sample are 5 × 10<sup>14</sup>/cm<sup>2</sup> for carrier concentration, 45 cm<sup>2</sup>/Vsec for mobility, 269 ohm/square for sheet resistance and 2-25 micron for the grain size. Laser annealing increases the mobility in a dramatic manner. For this large grain size in the heavily doped layer, the grain boundary scattering is negligible as compared to impurity scattering and conductivity is the same as that expected from a single crystal.

## DEVICES

### MOS Devices

MOS structures formed by implanting 185 keV Arsenic to a dose of 1 × 10<sup>16</sup> ions/cm<sup>2</sup> through a 700 Å gate oxide (Fig. 7) were pulse annealed<sup>5</sup> through the oxide. The leakage current at 5V bias was 30 picoamps as compared to 18 picoamps in thermally annealed diodes. C-V curves of a typical ion

implanted pulse annealed MOS is shown<sup>5</sup> in Fig. 8. A 10 min thermal anneal at 450°C after E-beam annealing makes the structure practically free from any trace of damage. This anneal is typical of contacting process.

**Bipolar Transistors**

The characteristics of an implanted and pulse annealed transistor are shown<sup>5</sup> in Table 4. The base was formed by ion implantation through 0.6 micron thick oxide and the emitter, through window opening in 0.2 micron oxide. In some cases base width as low as 500 Å was achieved.

TABLE 4  
CHARACTERISTICS<sup>5</sup> OF TRANSISTORS WITH PULSED ELECTRON BEAM ANNEALED EMITTER IMPLANTS

Emitter Geometry (mils)	Beta	$BV_{ceo}$ (Volts)	$I_{ceo}$ (microamp)	$X_o$ ( $\mu\text{m}$ )	Base width ( $\mu\text{m}$ )
0.7x2.1	50-60	40	1.0	0.18	0.19

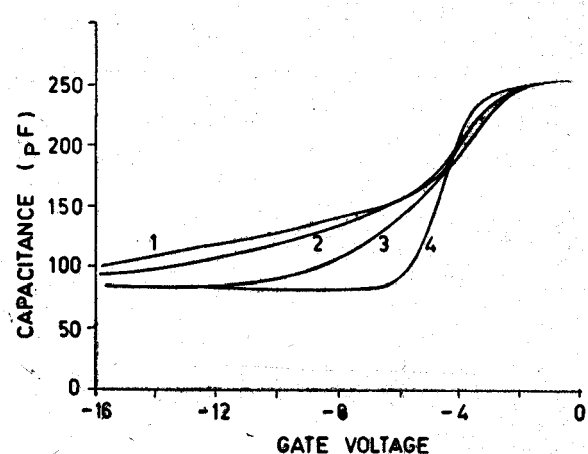


Fig. 8—Capacitance vs gate voltage plots of the implanted and pulsed electron beam annealed MOS diode. Curve 1, 2 and 3—after PEBA without heat treatment, curve 4—after PEBA plus 450°C alloy/anneal in  $H_2$ . Electron beam annealing followed by a few minutes of thermal annealing at 450°C removes practically all the defects.

**High Voltage Diode**

The break down voltage has shown great improvements in the recently implanted<sup>16</sup> diodes. The new techniques used for this purpose has a tapered oxide mask as shown in Fig. 9. The radius which determines the break down voltage varies as

$$= \frac{\text{Const}}{\tan \alpha}$$

The tapering is achieved by implanting Argon in top oxide layer so that it etches preferentially as shown in Fig. 9.

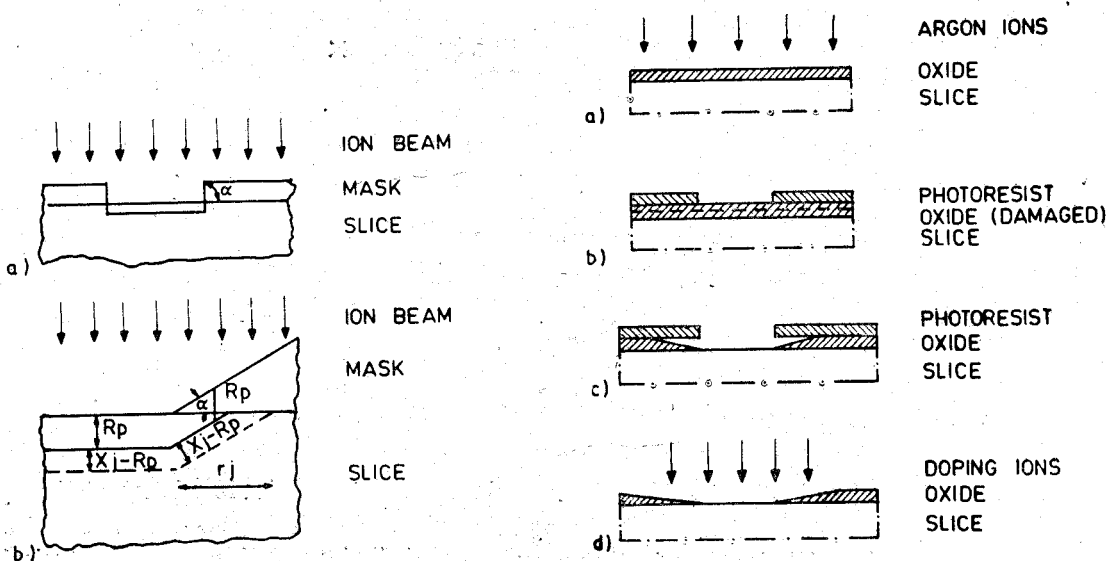


Fig. 9—Schematic procedure used to fabricate high voltage implanted diodes.

Silicon Solar Cells

Many authors have studied<sup>5,13,17,20</sup> ion implanted and laser or E-beam annealed solar cells. Muller *et. al.* have fabricated<sup>17,19</sup> an inexpensive ion implanter for fabricating solar cells at low costs. In this ion implanter (Fig. 10) a glow discharge is established in a glass chamber containing a mixture of carrier gas and a gas containing the dopant (e.g.  $PF_5$ ) at  $10^{-2}$ — $10^{-3}$  Torr. A stable plasma is created by adjusting the d.c. voltage (approximately 6 kV) across the gas mixture. Ions are extracted from this plasma and accelerated towards the sample at 30 kV. No mass separation is performed. Solar cells were fabricated using a total dose of  $10^{16}$  ions/cm<sup>2</sup>. Damage due to implantation was annealed using laser beams and cells upto 10 percent efficiency on EFG ribbons were made.

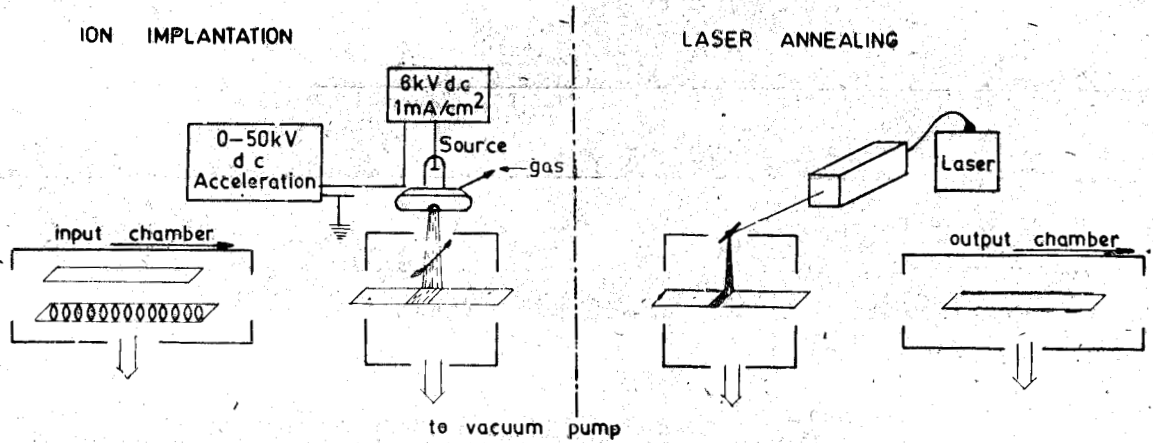


Fig. 10—Schematic diagram of an inexpensive Ion Implanter to make low cost high efficiency solar cells on EFG silicon ribbons.

Solar cells on 76 mm diameter wafer have been recently fabricated by implanting 5 keV phosphorus to a dose level of  $1 \times 10^{16}/\text{cm}^2$  and then annealing by single electron beam pulse<sup>5</sup>. Efficiency of 15 percent was achieved in a routine manner. Fogarassy *et. al.* annealed<sup>12,13</sup> the diffused solar cells using multimode pulsed ruby laser in the range 0.8 to 2 J/cm<sup>2</sup> and pulse width of 20 to 35 ns. The diffusion was done using  $POCl_3$ . The front grid was of evaporated 1000 Å of aluminium and back contact was of pure gold. Fig. 11 shows the effect of laser annealing on the short circuit current and open circuit voltage of the typical cell. A commercial cell was also irradiated with the laser beam of 1.1 J/cm<sup>2</sup> by Fogarassy *et. al.* The improvement in the I = V curve and in the efficiency of this cell is shown in Fig. 12.

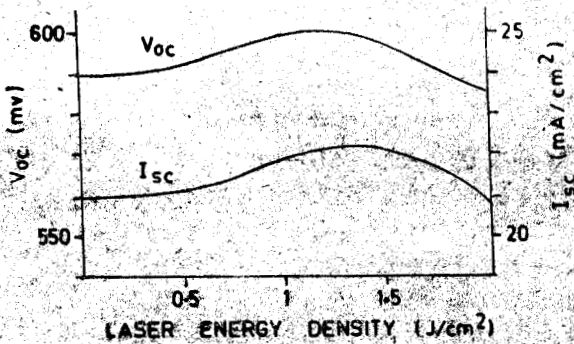


Fig. 11—Changes in the open circuit voltage  $V_{oc}$  and short circuit current  $I_{sc}$  of implanted solar cells are shown as a function of energy of the annealing laser pulse.

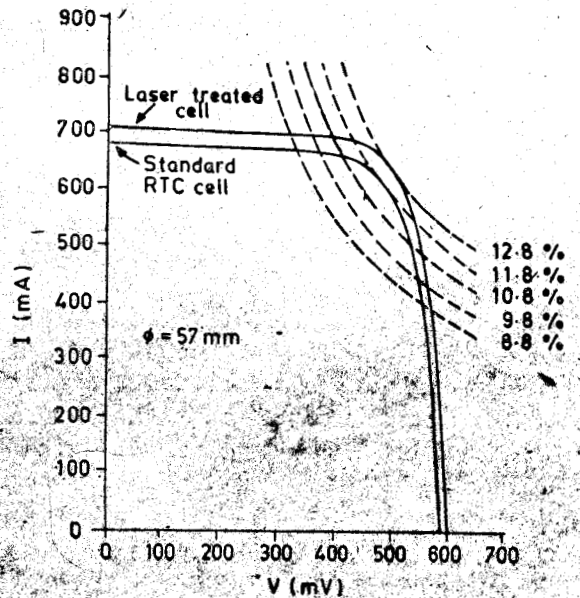


Fig. 12—Effect of laser annealing of a standard commercial cell. Both short circuit current and the open circuit voltage have increased and efficiency has gone up from 11.8 to 12.8 percent.

The increase in the short circuit current (Fig. 11) is due to both reduction in the series resistance and improvement in the collection efficiency. The increase in open circuit voltage appears to be due to the increase in active phosphorus concentration in diffused layer. The decrease in the voltage and the current on increasing the energy of the laser beam is presumably due to increased junction depth and/or due to introduction of some point defects in the base of the cell. Spectral response measurements in the implanted cells show<sup>18</sup> that on laser annealing the response on the IR side decreases, as shown in Fig. 13. Further work is necessary for better understanding of this effect.

Due to various improvements and new developments, the cost of solar cells made by implantation and annealing is likely to come down significantly. Results of a recent study<sup>20</sup> on cost calculation are shown in Table 5.

TABLE 5  
APPROXIMATE COST EVALUATION (Rs/W) FOR THREE DIFFERENT PROCESS OF SOLAR CELL FABRICATION<sup>20</sup>

Process of solar cell fabrication	Efficiency	
	11%	15%
Process I (Ion implantation+Thermal annealing)	10	7
Process II (Ion implantation+Laser annealing or Electron beam annealing)	3	2
Process III (Diffused junction)	11	8

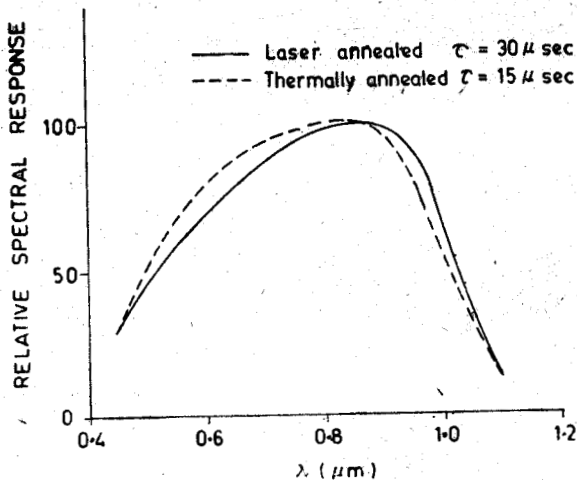


Fig. 13—Effect of laser annealing on the relative spectral response of a implanted solar cell.

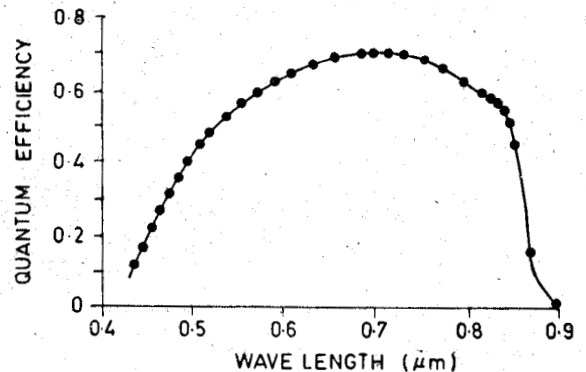


Fig. 14—Quantum efficiency or spectral response of an implanted and laser annealed GaAs solar cell.

### Gallium Arsenide Devices

Though bulk of the work has been done on silicon layers and devices, a few papers published recently<sup>5,21</sup> show that E-beam annealing has great potential in Gallium Arsenide (*GaAs*) and other III-V compound devices. In addition to the advantages of E-beam annealing mentioned earlier, there is an additional advantage in the case of *GaAs*. For thermal annealing, the implanted sample has to be heated to 900°C for 5–15 min and to avoid loss of *As*, *GaAs* has to be encapsulated. In E-beam annealing, the defects are removed in a very short time and therefore no encapsulation is required. Recently *GaAs* solar cells have been made<sup>21</sup> utilising a shallow homojunction  $n^+/p/p^+$  structure without *GaAlAs* window. The  $n^+$  layer was formed by  $Se^+$  ion implantation and annealed by a CW *Nd*:YAG laser. 12 percent efficiency at A1 Air Mass was achieved.

Quantum efficiency as a function of wavelength for a typical *GaAs* cell is shown in Fig. 14. The efficiencies are lower than those of the best cell (*GaAlAs* window, 20 percent efficiency) by about 20 percent. This work is in early stages of development, but the promise is high. Even a 12 percent efficiency without *GaAlAs* window is a significant achievement. Optimising implantation and annealing parameters are bound to yield considerable improvement. There does not appear to be any obstacle in developing 20 percent cells and at a much lower cost, using ion implantation and E-beam annealing methods.

LIFETIME MEASUREMENTS

If the emitter  $n^+$  is heavily doped, the contribution of the emitter to the forward current is small and in most cases it can be neglected. This approximation, originally used for the steady state, was extended to the time dependent case rather unfortunately. The open circuit voltage decay (OCVD) and Reverse Recovery methods of measuring the lifetime  $\tau$  based on this approximation were developed. Tewary and Jain<sup>22</sup> have recently shown that this approximation in the time dependent case leads to unusual results. The correct interpretation of the observed results is rather involved and it is difficult to get the accurate values of lifetime in a simple manner from these measurements.

A method to determine the lifetime  $\tau$  experimentally in both the  $n$  and  $p$  layers using an electron beam was suggested many years ago<sup>6,7&8</sup>. However, until recently the technique remained rather crude and gave only rough values. Recently the technique has been perfected to an extent that the values of  $\tau$  at different depths from the surface in  $n^+$  or  $p$  layer can be accurately determined.

When an electron beam enters a semiconductor, it creates a concentration  $N$  of electron hole pairs which decays roughly exponentially with distance from the point of primary impact. Shea, Partain and Warter<sup>6</sup> have shown recently that  $N$  is given by

$$N = \exp \left( -\frac{Y}{0.2R_B} \right), \text{ when } 0.1 R_B < Y < 0.5 R_B$$

and 
$$N = \text{Const } e \left( -\frac{Y}{0.1R_B} \right), \text{ when } 0.5 R_B < Y < R_B$$

$$N = 0; \text{ when } Y > R_B$$

The range  $R_B$  is given by

$$R_B = \text{Const } E_0^n \text{ micron}$$

where  $E$  is the energy of the electron beam and  $N = 1.62$  for  $\text{Cu}_2\text{S}$  and  $\text{CdS}$  and  $1.75$  for silicon.

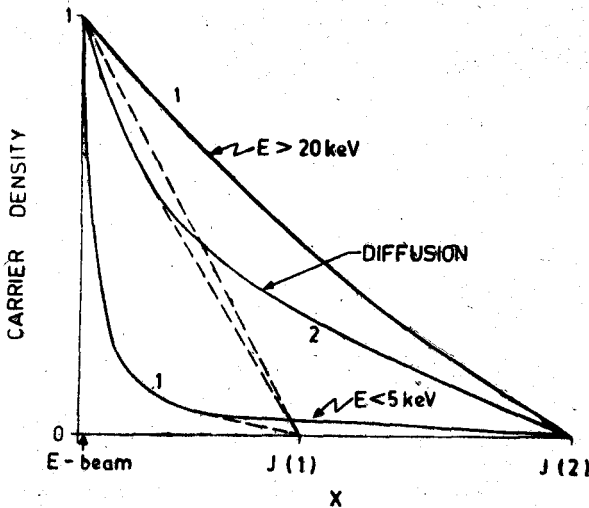


Fig. 15—Schematic carrier distribution profiles produced by the electron beam at  $x=0$  between  $x=0$  and the junction position  $J$ . are shown Profiles 1 secondary carrier density are established due to the secondary carrier production by the impact of the primary beam. Profile 2 is established due to the diffusion of carriers from the point of production  $x=0$  to the junction position  $J$ . If the energy of the incident beam is low, secondary carriers are confined to the close neighbourhood of  $x=0$  and the diffusion length can be obtained by measuring the short circuit current which is mainly due to the diffusion of carriers to the junction. When the energy is high, the secondary carrier density near the junction is higher than the carrier density due to diffusion and the diffusion length under these conditions cannot be measured.

For silicon,  $R_B$  is 0.125 micron at 3 keV, 1.03 micron at 10 keV and 7.06 micron at 30 keV.

Consider the case where an electron beam enters at  $x=0$  and makes primary impact to create electron hole pairs. The profiles of these carriers for very small energy of incident beam is shown by curve 1 (for  $E < 5$  keV) Fig. 15. It is seen from this curve that the charge carriers created by the electron beam are confined to a small vicinity of the beam and its concentration falls very rapidly in moving towards the junction shown at two positions  $J(1)$  and  $J(2)$  from the beam. These carriers diffuse to the junction and a diffusion profile shown by curve 2 is established. If the distance  $J$  is sufficiently large, the short circuit  $I_{sc}$  is given by

$$I_{sc} = \text{Const } e^{-J/L}$$

where  $L$  is the required diffusion length and can be easily determined from a plot of  $\ln I_{sc}$  vs.  $J$ . However if  $E$  is large the profile of the carriers produced by the beam is shown by curve 1, ( $E > 20$  keV). The short circuit current  $I_{sc}$  is now determined by this profile and diffusion of carriers does not play any significant role. It will be seen

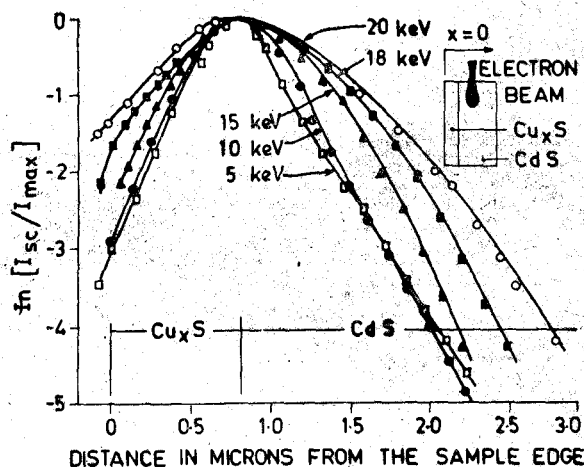


Fig. 16—Short circuit current as a function of the distance of the primary electron beam from the junction in copper sulphide-cadmium sulphide solar cells. Note that for small energy values, the plots are independent of the energy and these plots can be used for determining the diffusion length as explained in Fig. 15. When the energy of the beam is high, the short circuit current depends strongly on this energy.

that this technique will give good results for  $L$  only at low values of  $E_0$  such that  $R_B$  is considerably smaller than  $L$ . Experimental results for  $CuS_x : CdS$  Solar Cells of Shea *et. al.*<sup>6</sup> are shown in Fig. 16. It is seen that for  $E=5$  keV and 10 keV, the plots are independent of  $E$  and slope gives the values of  $L$ . For larger values of  $E$ , the slope depends on  $E$  and the slopes of the plots do not give values of  $L$  directly.

Possin and coworkers<sup>7,8</sup> have extended this technique to study lifetime and damage due to ion implantation in silicon as a function of depth from the surface. Since lifetime is a sensitive function of the radiation damage, damage profile can be studied by this method.

#### ACKNOWLEDGEMENT

The help of Shri P. K. Basu in preparing this manuscript is gratefully acknowledged.

#### REFERENCES

1. U.S. PATENT 3,950,187, (1974).
2. KACHURIN, G.A., PRIDACHIN, N.B. & SMIRNOV, L.S., *Sov. Phys. Semicond.*, **9** (1975), 946.
3. KIRKPATRICK, A.R., MINNUCCI, J.A. & GREENWALD, A.C., *IEEE, Trans. Elec. Devices ED-24* (1977), 429.
4. GIBBONS, J.F., GAT, A., GERZBERG, L., LIETOILA, A., REGOLINI, J.L., SIGMON, T.W., PEASE, R.F.W., MAGEE, T.J., PENG, J., HONG, J., DELINE, V., KATZ, W., WILLIAMS, P. & EVANS, C.A., (unpublished) See also, GIBBONS, J.F., paper presented at the 15th Symposium on Electron, Ion and Photon Beam Technology, Boston (May/June 1979).
5. GREENWALD, A.C. & LITTLE, R.G., *Solid State Technology*, **22** (1979), 143.
6. SHEA, S.P., PARTAIN, L.D. & WARTER, P.J., *Scanning Electron Microscopy*, **1** (1978), 435.
7. POSSIN, G.E., ADLER, M.S. & BALIGA, B.J., paper presented at the American Society for Testing Materials Conf. on Lifetime in silicon, San Diego, Calif., Feb (1979).
8. POSSIN, G.E. & KIRKPATRICK, C.G., paper presented at 15th Symposium on Electron, Ion and Photon Beam Technology Boston (May/June 1979).
9. Papers presented at the 15th Symposium on Electron, Ion and Photon Beam Technology Boston (May 29-June 1, 1979).
10. 'Update on free electron lasers and application', *Physics Today* **32**, No. 7, 19 (July 1979).
11. SHAVER, D.C., FLANDERS, D.C., Ceglie, N. M. & HENRY I. SMITH, paper presented at the 15th Symposium on Electron, Ion and Photon Beam Technology, Boston (May/June 1979).
12. FOGARASSY, E., STUCK, R., MULLER, J.C., GROB, A. and J.J. & SIFFERT, P., paper presented at the 21st Electronic Materials Conference, Boulder (June 1979).
13. FOGARASSY, E., STUCK, R., MULLER, J.C., GROB, A. and J.J., SIFFERT, P., SALLES, Y. & DIGUET, D., paper presented at the 1979 Photovoltaic Solar Energy Conference, Berlin (West), (April 1979).
14. See reference 4, pp 9-10.
15. GEIS, M.W., FLANDERS, D.C. & HENRY I. SMITH, *Applied Physics Letters* (July 1, 1979).
16. ZANDVELD, P. *Solid State Electronics*, **19** (1976), 659.
17. MULLER, J.C., GROB, A. and J.J., STUCK, R. & SIFFERT, P., paper presented at the Thirteenth IEEE Photovoltaic Specialists Conference, Washington (June 1978).
18. ZIGNANI, F., GALLONI, R., PEDULLI, L., BENTINI, G.G., SERVIDORI, M., CEMBALI, F. & DESALVO, A., paper presented at the International Conference on Solar Photovoltaic Energy, Berlin, (West), (April 1979).
19. BELL, R.O., HO, C.T., RAVI, K.V., WALD, F.V., MULLER, J.C. & SIFFERT, P., paper presented at the 1979 Photovoltaic Solar Energy Conference, Berlin (West), (April 1979).
20. ZIGNANI, F. & GALLONI, R., Technical Report, Research Contract No. 197-76-7 ESI, LAMEL-CNR Via Castagnoli, 1 Bologna, Italy.
21. JOHN, C.C. FAN, RALPH L. CHAPMAN, JOSEPHY P, DONNELLY, GEORGE W, TURNER & CARL O. BOZLER, *Appl. Phys. Lett.* **34** (1979), 780.
22. TEWARY, V.K. & JAIN, S.C. (to be published).